Geomechanics and Engineering, *Vol. 31, No. 2 (2022) 197-208*
https://doi.org/10.12989/gae.2022.31.2.197

Calculation method for settlement of micropile installed in rock layers through field tests

TaeHyun Hwang[a], JungMin Cho[b] and YeongSaeng Lee[*]

Department of Civil Engineering, Kyonggi University,
154-42, Gwanggyosan-ro, Yeongtong-gu, Suwon-si, Gyeonggi-do, Republic of Korea

(*Received July 25, 2022, Revised October 11, 2022, Accepted October 18, 2022*)

Abstract. Micropiles consisting of steel bars and grouts are commonly used in underpinning methods to reinforce supports or to suppress the subsidence of existing structures. Recently, applications in the field of geotechnical engineering have expanded. Despite the increasing use of micropiles are used, the PHC or steel pile formula is still applied for the settlement amount of micropiles. Compared with field test results, the amount of micropile subsidence obtained from the existing method may result in a very large error in the displacement of the micropile. Therefore, it is difficult to utilize micropiles effectively. Hence, to solve this problem, this study evaluated the behaviors and support characteristics of micropiles through field compression and tensile tests, and proposed a method for predicting the amounts of their subsidence. To confirm the appropriateness of the proposed method, field test results and the results obtained using the proposed method were compared. It was found that the settlement amounts of the micropiles as predicted through the existing method were significantly overestimated (error ≈ 50–80%) relative to the field test results, whereas the settlement errors of the piles predicted through the proposed method decreased (error ≈6–32%). Thus, it is possible to reduce the previously overestimated amount of settlement, and the modified method of this study allows more efficient design than the conventional method.

Keywords: behavior and bearing characteristic of pile; estimating method of micropile settlement; field test; micropile

1. Introduction

A micropile with a diameter of 300 mm or less does not require a large working space for pile construction, and the bearing capacity of pile is similar to that of the existing pile, such as an RC(Reinforced concrete) or PHC(Pretensioned spun high strength concrete)pile. Therefore, a micropile method as one of the underpinning methods has been applied for reinforcing the bearing capacity or suppressing the settlement of existing buildings. In addition, this method has recently been used to supplement the bearing capacity of structures and seismic retrofit methods (FHWA 2005, Wang *et al.* 2019, Capatti *et al.* 2020, EI Kamash *et al.* 2020).

With the increasing utilization of micropiles, many researchers have conducted studies on the support and behavior characteristics of micropiles. FHWA (2005) reported that the load worked on the micropile head was transferred in the order of steel bar, grout, and ground. Gómez *et al.* (2005) and Veludo *et al*. (2012) reported that the bond strength of micropile occurring at boundary of the steel bar/grout dependent on the installation diameter of the micropile and the bond strength to the existing foundation-concrete. Han and Ye (2006) reported that the bearing characteristics of micropile were greatly dependent on the bond strength occurring at the boundary of the ground/pile located in the upper pile through field tests.

Furthermore, the bearing capacity and settlement of the micropile are closely related to the area ratio of the steel bar and the grout. According to the study results of EI Kamash and Han (2017), it was found that the settlement of the footing was affected by the transferred load in the micropile, and the skin friction on the shaft of the micropile. Hwang *et al*. (2017a, b) reported that the bearing capacity and settlement of the micropiled raft were closely related to the fracture behavior, installation diameter and length of the micropile. According to a study of Moradi *et al.* (2021), the relative density of the adjacent soil of the pile is an important factor in increasing the bearing capacity of the micropile. As a result, experiments with sandy soils of varying relative densities revealed that increasing installation diameter was 12% more effective than increasing installation length.

As can be seen from the results of previous studies, when in the initial step a load is applied on the pile head, the steel bar resists the load. The load is transmitted in the order of the grout and the ground. In other words, it can be said that the main resistance to the load applied to the reinforcing bar. Also, due to the unique load transfer characteristics of the micropile, the bearing capacity and settlement amount of the micropile are closely related to the cross-sectional size of steel bar and grout as shown in Fig. 1.

When designing micropiles, the settlement amount of the micropile is obtained from the equation for the same settlement amount as that of a general pile, and the consideration factors

*Corresponding author, Professor
E-mail: yslee@kyonggi.ac.kr
[a]Adjunct professor
E-mail: makgohwang@hanmail.net
[b]M.S. Student
E-mail: chominit@kyonggi.ac.kr

ISSN: 2005-307X (Print), 2092-6219 (Online)

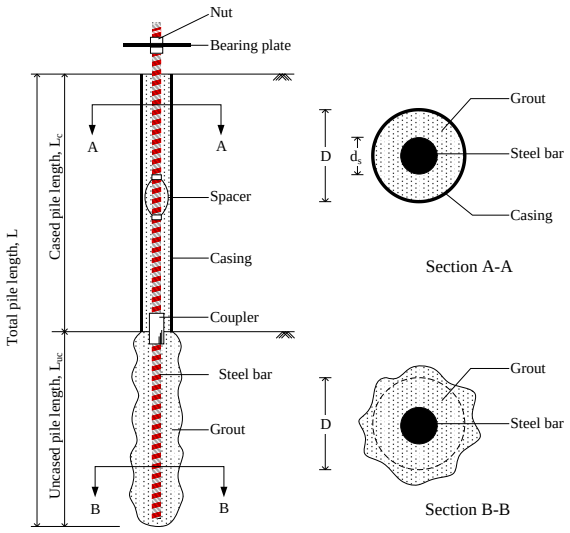

Fig. 1 Structure of micropile in a soil layer

for the micropile applied to this equation are the axial rigidity determined by the cross-sectional area and the rigidity of the steel bar and grout. That is, when calculating the amount of settlement, there is a problem in that the actual load transfer characteristics of the micropile are not being consideration. In addition, the settlement amount of the micropile calculated by the existing method has a large error compared to the settlement amount investigated through the field test. Thereby, in order to effectively utilize the micropile, a pile design considering the behavioral characteristics of the micropile will be required.

To solve this problem, this study proposed a method for calculating the settlement amount of micropile considering both the structural characteristics and the cross-sectional characteristics of the steel bar/grout. Also, evaluate the applicability of the proposed formula, the results obtained through the proposed method were compared with the test results performed in 6 regions in South Korea.

2. Settlement of Micropile

2.1 Micropile settlement calculation method

When designing a pile, as shown in Eq. (1), the total settlement amount of the pile is determined by the sum of the settlement amount of the pile structure and the settlement amount generated from the tip and peripheral area of the pile (Vesic 1977, Prakash and Sharma 1991, Das 2010).

$$\delta_t = \delta_{e(ES)} + \delta_{s(ES)} + \delta_{p(ES)} \quad (1)$$

δ_t is the total pile top settlement for a sing pile, $\delta_{e(ES)}$ is the settlement due to axial deformation of a pile shaft, $\delta_{s(ES)}$ is the settlement of pile point caused by load transmitted along the pile shaft. And $\delta_{p(ES)}$ is the settlement of pile base or point caused by load transmitted at the base.

A micropile is a small-diameter pile so Eq. (1) does not consider the amount of settlement at the tip of the pile. Therefore, it is possible to calculate the elastic settlement and the shaft settlement for the entire pile as shown in Eqs. (2) and (3), respectively.

$$\delta_{e(ES)} = \frac{P \cdot L}{E_{MP} \cdot A_{MP}} \quad (2)$$

$$\delta_{p(ES)} = \left(\frac{P}{\pi D L}\right)\frac{D}{E_s}(1-\mu_s^2)I_s \quad (3)$$

In Eqs. (2) and (3), P means the working load on the head of the micropile. E_{MP} and E_S are the moduli of the micropile and soil, respectively, and A_{MP} is the area of the micropile(= $\pi D^2/4$; D = diameter of the micropile). μ_s is the Poisson's ratio of the soil and I_S is an influence factor ($= 2 + 0.35\sqrt{L/D}$).

When calculating pile settlement using the method shown in Eq. (2), the settlement of the micropile structure considers only the axial rigidity of the micropile (E_PA_P), even though the steel bar is a major factor in resisting the working load. As can be seen from the results of previous studies, the supporting characteristics of micropiles are dependent on the cross-sectional area of the steel bars/grouts, which are also components of the pile. In addition, the load transfer characteristic of the pile is that the steel bar with the greatest material rigidity preferentially supports the working load, and the grout effectively resists the working load by restraining the steel bar. Thereby, it is reasonable to calculate the amount of settlement of the micropile based on the steel bar constrained by the grout. Since the restraining effect of the grout is different depending on the cross-sectional area and material rigidity, it would be reasonable to apply these characteristics.

2.2 Modified micropile settlement calculation method

The axial rigidity of the micropile was calculated by considering the axial rigidity values of the steel bar and grout, as shown in Eq. (4) (FHWA 2005).

$$E_{MP}A_{MP} = E_{ST}A_{ST} + E_GA_G \quad (4)$$

E_{ST} and E_G are the elastic moduli of the steel bar and grout, respectively. The elastic modulus of the grout (E_G) is equal to $4732\sqrt{\sigma_{ck}}$(MPa), where σ_{ck} is the unconfined compressive strength of the grout (FHWA, 2005). A_{ST} is the area of the steel bar(=$\pi \cdot d_{ST}^2/4$; d_{ST}= diameter of steel bar), and A_G is the area of the grout (=$A_{MP} - A_{ST}$). The total area of the micropile, A_{MP}, in Eq. (4) can be calculated through Eq. (5).

$$\begin{aligned} A_{MP} &= \frac{E_{ST}A_{ST}}{E_{MP}} + \frac{E_GA_G}{E_{MP}} \\ &= \frac{E_{ST}A_{ST}}{E_{MP}} + \frac{E_G(A_{MP}-A_{ST})}{E_{MP}} \\ &(\because A_{MP} = A_{ST} + A_G) \\ &= \left(\frac{E_{ST}}{E_{MP}} - \frac{E_G}{E_{MP}}\right)A_{ST} + \frac{E_G}{E_{MP}}A_{MP} \\ &= \frac{E_{ST}-E_G}{E_{MP}-E_G}\cdot A_{ST} \end{aligned} \quad (5)$$

Eq. (5) can be modified as in Eq. (6), and It can be seen that the axial stiffness, $E_{MP} \cdot A_{MP}$, of the micropile is related to the axial stiffness and cross-sectional area of the steel bar as shown in Eq. (6). Here, the coefficient m is defined as the ratio of the elastic modulus of the steel bar, grout, and micropile. The elastic modulus of the micropile, E_{MP}, is determined using Eq. (4).

$$E_{MP} \cdot A_{MP} = \left(\frac{1 - \frac{E_G}{E_{ST}}}{1 - \frac{E_G}{E_{MP}}} \right) \cdot E_{ST} \cdot A_{ST} \tag{6}$$

$$= m \cdot E_{ST} \cdot A_{ST}$$

In this study, through the test results shown in Fig. 9, it was confirmed that the steel bar is the main resistance supporting the applied load. Based on the study results, the modulus ratio, E_G/E_{MP}, in Eq. (6) was assumed as the modified elastic modulus ratio, $n \cdot (E_G/E_{ST})$, of the steel bar and grout as shown in Eq. (7). Where, n means a correction factor for the material stiffness ratio. This correction factor can be defined as a function of the axial stiffness ratio of the steel bar and the grout as shown in Eq. (8) and can be estimated through field test results.

$$\frac{E_G}{E_{MP}} = n \cdot \frac{E_G}{E_{ST}} \tag{7}$$

$$n = f\left(\frac{E_G \cdot A_G}{E_{ST} \cdot A_{ST}} \right) \tag{8}$$

In addition, the coefficient m in Eq. (6) can be defined as follows by substituting Eq. (8) into Eq. (6).

$$m' = \frac{1 - E_G/E_{ST}}{1 - nE_G/E_{ST}} = \frac{1 - R}{1 - nR} \tag{9}$$

The modified calculation method for the elastic settlement amount of the micropile structure considering the load transfer characteristics of the micropile can be derived as Eq. (10) by substituting Eq. (9) into Eq. (2). Then, the modified total settlement for the micropile can be calculated using Eq. (11).

$$\delta'_{e(MES)} = \frac{P \cdot L}{E_{MP} \cdot A_{MP}} = \frac{P \cdot L}{m' \cdot E_{ST} \cdot A_{ST}} \tag{10}$$

$$\delta'_t = \delta'_{e(MES)} + \delta_{p(ES)}$$

$$= \frac{P \cdot L}{m' \cdot E_{ST} \cdot A_{ST}} + \left(\frac{P}{\pi D L} \right) \frac{D}{E_s} (1 - \mu_s^2) I_s \tag{11}$$

The FHWA (2005) defined the allowable yield strength of a steel bar as the strength equivalent to a deformation rate of 0.03%. Das (2010) proposed that the maximum friction resistance on the shaft of the pile occurs when the relative settlement at the boundary of the ground/pile is 5–10 mm. Considering this, the relative displacement occurring on the shaft of the pile is larger than the elastic displacement of the micropile structure. Thus, considering that the micropile is a small-diameter pile, the displacement occurring on the shaft of the pile can be regarded as occurring beyond the elastic limit of the micropile. Thereby, it is appropriate to compare and analyze the settlement amount of the micropile structure with the elastic settlement in the field test results. it is appropriate to compare and analyze the amount of settlement that occurred on the shaft of the micropile with the plastic settlement in the field test results.

In addition, the amount of shaft settlement is related to the skin friction characteristics of the ground/pile. Hence, it is unclear whether in Eq. (11), the pile length should be applied to the total length, L_T (=L_c+L_{uc}; Fig. 1), of the pile or the uncased length, L_{UC}. This is because the FHWA (2005) considered the skin friction characteristics of the ground and grout (which correspond to the adhesive length) when calculating the skin friction force of the pile, whereas the French design code "CCTG" (1992) considered the total length of the pile containing the cased length (L_c). Therefore, when estimating the settlement amount for the pile shaft, the pile length applied in Eq. (11) is the total pile length and the bonded length.

3. Field tests of micropile

3.1 Ground conditions for each site

The field compression and tensile tests for the micropiles were conducted in six regions of Seoul, Daegu, and Incheon, as shown in Fig. 2(a). The site ground conditions were evaluated using the Standard Penetration Test (SPT) and the Unified Soil Classification System (UCSC). The sediment layers of sites 1 and 4–6 sediment layers comprised GP-GW, SW-SM, SP, and SM assemblies (granular soil), as shown in Fig. 2(b).

In the case of sites 2 and 3, the upper sediment layer is CL-ML and/or ML fine-grained soil, and the SPT results show that the density of this ground is soft soil between N=1/30 and 4/30. In addition, a GW-GM layer with a thickness of approximately 3 m exists in the lower ground and SP (Sand Poor) assembly ground (Grand soil layer).

The rock layers at all sites are located at the bottom of the sediment layer, as shown in Fig. 2(b). The geological conditions for the bedrock were weathered rock at all sites except sites 4 and 5. And the SPT results show that they comprise a weathered rock layer (WR) at N ≥ 50/10. The bedrock layer at sites 4 and 5 is a soft rock layer (soft rock layer, SR) with a rock quality designation of 8–15%.

3.2 Micropile conditions for each site

The diameter and length of the micropile installed in the ground are determined from Eqs. (12) and (13) (FHWA, 2005).

$$P \leq \frac{\alpha(\pi D L_{uc})}{F.S} \tag{12}$$

$$P \leq \{0.4\sigma_{c(G)} A_G + 0.47\sigma_{y(S)} A_{ST}\} \tag{13}$$

In the above, α is the ultimate bond strength at the interface of the grout and ground, $\sigma_{c(G)}$ is the unconfined compressive strength of the grout (typically the 28-day strength), $\sigma_{y(S)}$ is the yield stress of steel, and F.S is a safety factor for the ultimate bond strength (F.S ≥ 2.0; typically, F.S = 2.5).

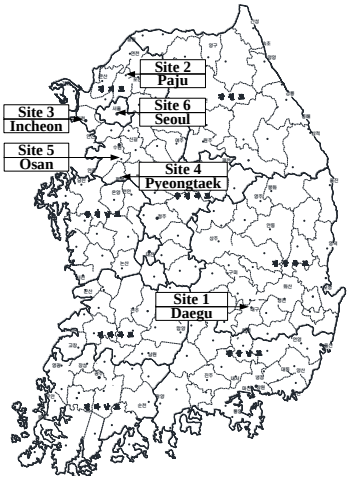

(a)

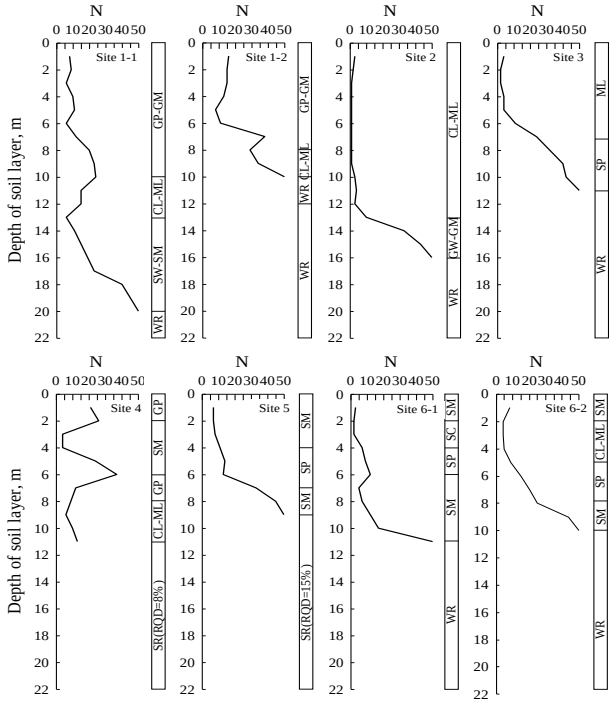

(b)

Fig. 2 Test site and conditions of soil layers : (a) Test site and (b) Soil conditions

Table 1 Pile diameter and field test type of micropile for each site

Site	Diameter of micropile (m)		α (kPa)	Bearing capacity, P_a (kPa)	Test load, P_{TC} or P_{TE} (kN)		Field test type
	Pile	Steel bar			Compress	Tension	
Site 1-1	0.20	0.05	215	270.18	560	560	Compression/Tension
Site 1-2	0.20	0.05	215	270.18	560	560	Compression/Tension
Site 2	0.15	0.05	300	282.74	720	-	Compression
Site 3	0.15	0.065	400	254.47	440	-	Compression
Site 4	0.15	0.065	450	414.69	1,570	-	Compression
Site 5	0.20	0.075	450	678.58	1,415	-	Compression
Site 6-1	0.20	0.075	400	565.49	1,275	-	Compression
Site 6-2	0.20	0.075	400	565.49	1,275	1,275	Compression/Tension

Fig. 3 shows the pile length for each site shown in Fig. 2. The pile length installed at each site was determined using Eq. (12). Where, α is the bond strength per unit area, and this design value is proposed by Xanthakos(1991) and FHWA(2005). When determining the diameter of the micropile through Eq. (13), the yield strength of the steel bar (steel grad 500/550) and grout(= $4732\sqrt{\sigma_{ck}}$ and σ_{ck}=24MPa) and the allowable bearing capacity of the pile (Table 1) were considered.

3.3 Field compression and tension tests

The micropiles were installed in the order of the casing installation, boring, steel bar insertion, and grout. The casing was installed to prevent collapse of the bored hole.

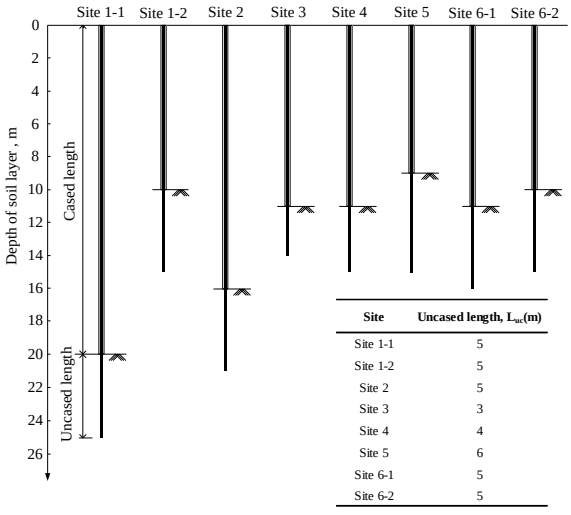

Site	Uncased length, L_{uc}(m)
Site 1-1	5
Site 1-2	5
Site 2	5
Site 3	3
Site 4	4
Site 5	6
Site 6-1	5
Site 6-2	5

Fig. 3 Installed length of micropile for each site

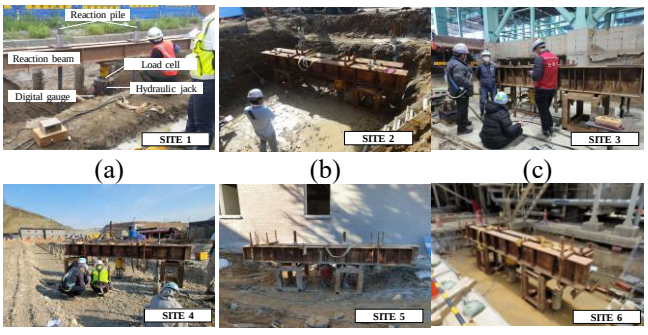

(a) (b) (c)

(d) (e) (f)

Fig. 4 Photography of field compression test: (a) Site 1, (b) Site 2, (c) Site 3, (d) Site 4, (e) Site 5 and (f) Site 6

The grouting method was the gravity grout (Type-A). After hardening the grout for 28 days, field tests were performed. A full view of the compression tests conducted at sites 1-6 is shown in Fig. 4. The field tests shown in Fig. 4 complied with the test procedure suggested by FHWA (2005). In the case of sites 1-5, the process of loading and unloading was performed while applying the load step by step on the pile head to measure the elastic and plastic displacement of the pile. On the other hand, in the case of site 6, the compressive load was gradually increased until the final step. The test load was applied using a hydraulic jack and load cell installed between the reaction beam and the head of the test pile, as shown in Figs. 4(a)-4(f). The compressive load of each stage was maintained for the duration until the generated displacement of the pile by the test load became constant.

The maximum test load for the compression test, $P_{TC(max)}$ is equal to or more than twice the allowable bearing capacity P_a of the pile. These results are shown in Table 1 ($P_{TC(max)} \geq 2 \cdot P_a$). The magnitudes of the test load applied at each step were equal to 25, 50, 75, and 100% of the maximum test load. The magnitude of the test load and the compression displacement of the pile were measured using a load cell installed on the head of the pile and a digital displacement measuring instrument as shown in Fig. 4(a).

(a) (b) (c)

Fig. 5 Photography of field tension test: (a) Site 1-1, (b) Site 1-2, (c) Site 6-2

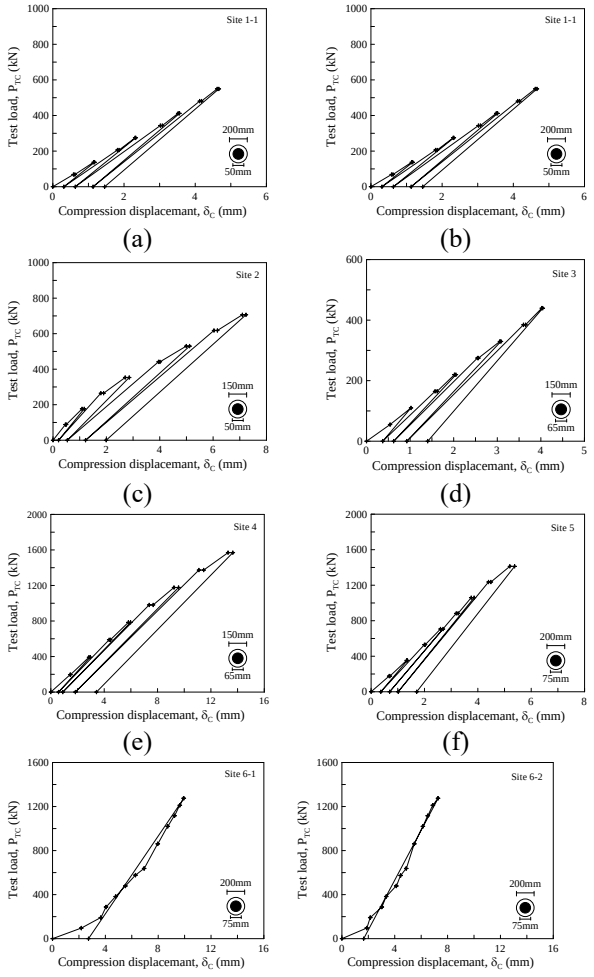

(a) (b) (c) (d) (e) (f) (g) (h)

Fig. 6 P_c-δ_c relation in results of field compression tests: (a) Site 1-1, (b) Site 1-2, (c) Site 2, (d) Site 3, (e) Site 4, (f) Site 5, (g) Site 6-1 and (h) Site 6-2

The field compression and tensile tests were conducted at sites 1 and 6-2 as shown in Figs. 4(a), 4(f), and Fig. 5. The field tensile test process also followed the test process presented by the FHWA (2005). The method of loading the tensile test in this study gradually increased the load until the final test step, and the load was applied to the head of the pile. As shown in Fig. 5(a), the test load material was applied step-by-step using a hydraulic jack and load cell installed on the reaction beam.

The tensile load at each stage was maintained for the duration time until the displacement of the pile was converged, and the test load was increased after the displacement of the pile was converged. The magnitude of the maximum test load applied to the pile during the test

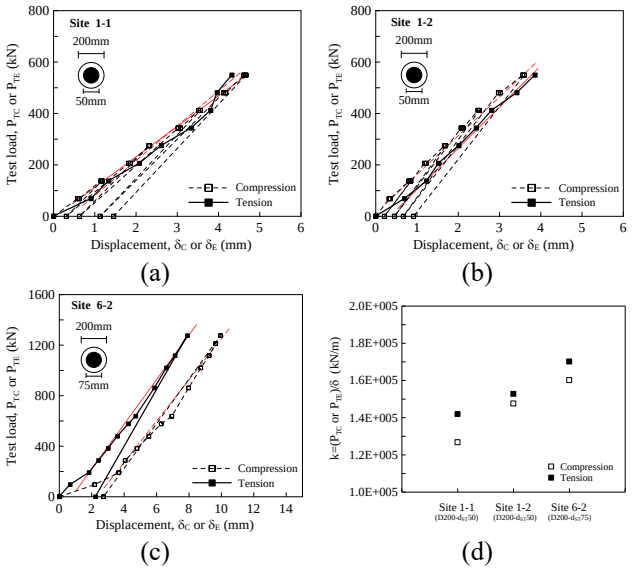

Fig. 7 Comparison of compression and tension test results: (a) Site 1-1, (b) Site 1-2, (c) Site 6-2 and (d) Comparison of k(=P/δ) for each site

was more than twice the allowable bearing capacity of the pile $P_{TC(max)}$ and $P_{TE(max)} \geq 2 \cdot P_a$; Table 1). The compression and tensile displacement of the pile were measured using a load cell installed on the head of the pile and a digital displacement measuring instrument as shown in Fig. 5(c).

4. Results of field test

4.1 Load-displacement of micropile in field test

Fig. 6 shows the load-displacement relationships of the micropile investigated through field tests for each site. As shown in Fig. 6(a) through 6(h), the total displacement of the pile in the final load step was 3.3–14.2 mm, and the displacement of the micropile which installed at site 4 was measured to the maximum. Furthermore, the compression and tensile load-displacement relationships of the micropiles investigated at site 6 were similar, as shown in Figs. 6(g)-6(h).

Fig. 7 compares the relationship of displacement to compressive and tensile loads investigated at site 1 and site 6-2. Where, δ_{TC} and δ_{TE} means the compression and tension displacement of pile obtained from field tests. The difference in displacement between the compressive and tensile displacements of the piles for each load step was about 0.5 mm in the case of site 1, and about 2.0 mm in the case of site 6-2, as shown in Fig. 7(a) and 7(b). These results indicate that the micropiles have similar resistance to compressive or tensile loads, and the micropiles are supported by the pile structure and skin friction.

On the other hand, the gradient k(= (P_{TC} or P_{TE}) /δ) of the load-displacement graph at each site was about 1.27×10^5–1.70×10^5 kN/m, and the gradients were similar. This comparison means that the resistance of the micropile to the applied load depends on the specific material properties of the pile, as mentioned in FHWA (2005). it can

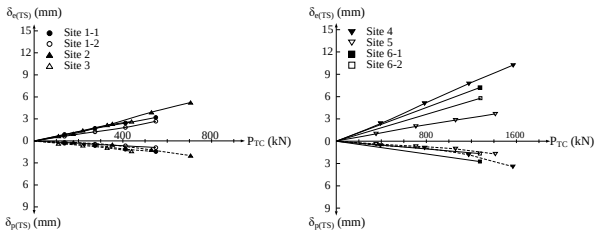

Fig. 8 Elastic and plastic displacement with compression load: (a) Sites 1–3, (b) Sites 4–6

be said that the steel bar is the main resistance in the constituent material of the micropile.

Fig. 8 shows the elastic and plastic displacement of the micropile investigated through the load-displacement relationship of Fig. 6. The maximum elastic displacement (max. $\delta_{e(TS)}$) of the micropile investigated at sites 1-3 was 2.69-5.25 mm, as shown in Fig. 8(a), and the displacement of the pile as the load increased tended to increase linearly. Also, the maximum plastic displacement (max. $\delta_{p(TS)}$) was 0.92–1.99 mm, the plastic displacement of pile according to the increase of the test load also showed a tendency to increase linearly. The elastic displacement of the micropile investigated at sites 4-6 was 3.67-10.22 mm, and the plastic displacement was 1.65-3.42 mm, as shown in Fig. 8(b).

The elastic displacement of the micropile investigated at sites 4-6 was 3.67-10.22 mm, and the plastic displacement was 1.65-3.42 mm, as shown in Fig. 8(b).

4.2 Bearing behavior of micropile

Fig. 9 compares the relationships of max.$\delta_{e(TS)}$-P_{TC}, max.$\delta_{e(TS)}$–L/D, max.$\delta_{e(TS)}$-D and max.$\delta_{e(TS)}$-d_{ST} investigated by site. The maximum elastic displacement was 2.69-10.22 mm, as shown in Fig. 9(a), and it occurred at site 4, where a test load of 1570 kN was applied. Fig. 9(b) compares the maximum elastic displacement according to the pile length ratio L/D, and the comparison results show that the elastic displacement of the pile is not significantly affected by the pile length ratio. In the case of sites 1-1 and 1-2, there was a large difference in pile length ratio, but the maximum elastic settlement that occurred in the pile body was similar. In addition, in the case of sites 5 and 6, the maximum elastic displacement that occurred in the test piles at site 6 was small even when a large test load was applied.

Figs. 9(c) and 9(d) compare the maximum elastic displacement of the micropile according to the diameter of the pile and steel bar. As a result of comparison, as shown in Fig. 9(c) and (d), the maximum elastic displacement of the pile increased as the diameter of the pile or steel bar was small, and the magnitude of the load increased. These results show that, as suggested by Moradi *et al.* (2021), the bearing capacity of the micropile is more dependent on the change in the pile diameter than the change in the pile length ratio. In addition, through the test results of this study, it shows that it is more dependent on the diameter of the steel bar rather than the change in the overall diameter of the pile (Fig. 9(d)).

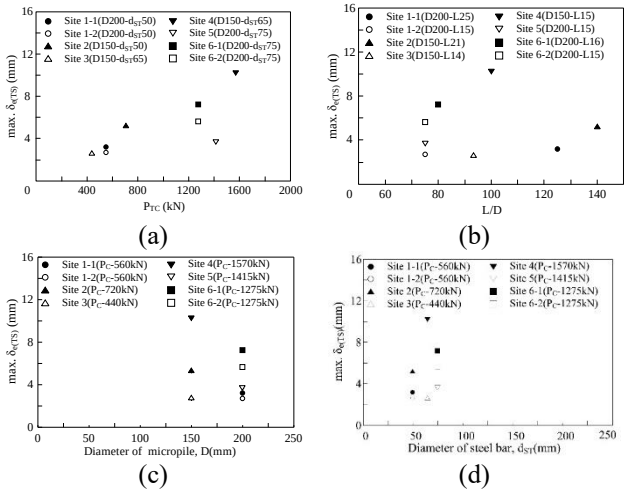

Fig. 9 Max. elastic displacement by P_{TC}, L/D, D and d_{ST}: (a) max.$\delta_{e(TS)}$-P_{TC}, (b) max.$\delta_{e(TS)}$–L/D, (c) max.$\delta_{e(TS)}$-D and (d) max.$\delta_{e(TS)}$-d_{ST}

Fig. 10 compares the maximum plastic displacement of micropile ($\max.\delta_{p(TS)}$) according to the compression test load (P_{TC}), pile length ratio (L/D), and uncased length ratio(L_{uc})/D). The maximum plastic displacement of the micropile investigated through the field test was 1.46-3.42 mm (Fig. 10). As shown in Figs. 10(a) and 10(b), the maximum plastic displacement of the piles investigated at each site was similar regardless of the magnitude of the applied load and the pile length ratio.

It should be noted that the diameter of the micropiles at each site was different, but the bonded length of the micropiles was similar (Fig. 3). And as shown in Fig. 10(c), the plastic displacement of micropiles according to L_{uc}/D, which is defined as the ratio of bonded length and diameter, is similar. The results of this study show that the plastic displacement of micropiles occurring at the pile/ground boundary is closely related to the bonded length, L_{uc}, in the length of the micropile. Therefore, it is judged that it is reasonable to consider the bonded length for settlement caused by the load carried on the shaft of the micropile.

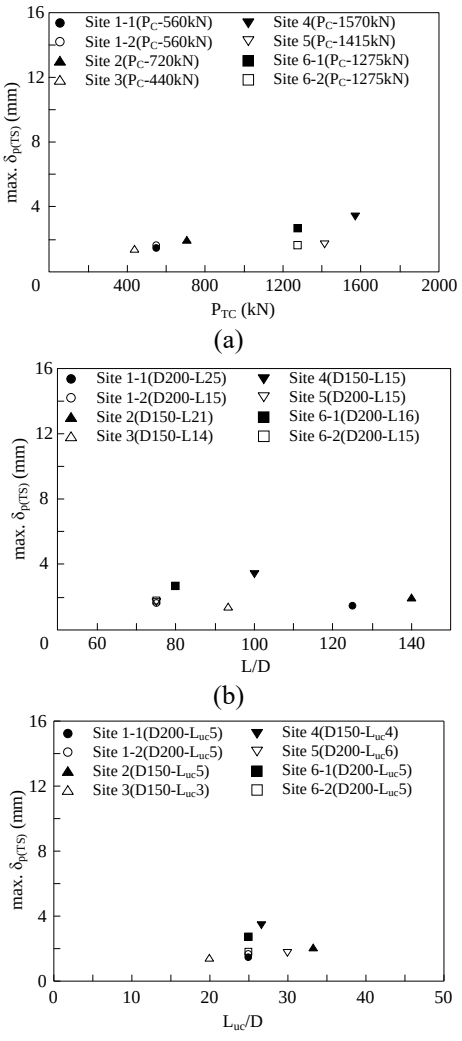

Fig. 10 Max. plastic displacement by P_{TC}, L/D and L_{uc}/D: (a) max.$\delta_{p(TS)}$ - P_{TC}, (b) max.$\delta_{p(TS)}$– L/D and (c) max.$\delta_{p(TS)}$–L_{uc}/D

5. Settlement of micropile

5.1 Comparison test results with the settlement of Eq. (2)

Fig. 11 shows the result of comparing the settlement amount of the micropile obtained through Eq. (2) with the amount of elastic displacement obtained from the field test (P_C-$\delta_{e(ES)}$ or $\delta_{e(TS)}$). As a result of the comparison, the settlement amounts of the pile obtained through Eq. (2) are significantly overestimated than compared to that of the micropile investigated through the field compression test.

Table 2 compares the error between the elastic settlement amounts of micropiles investigated through the test results and the elastic settlement amounts of micropiles obtained through Eq. (2). It can be seen that the error of the two results was 51.4-78.6%, which is very large. That is, it can be said that it is inappropriate to predict the elastic displacement between the micropile composed of the grout and the steel bar through the existing estimated method, Eq. (2), based on the comparison results.

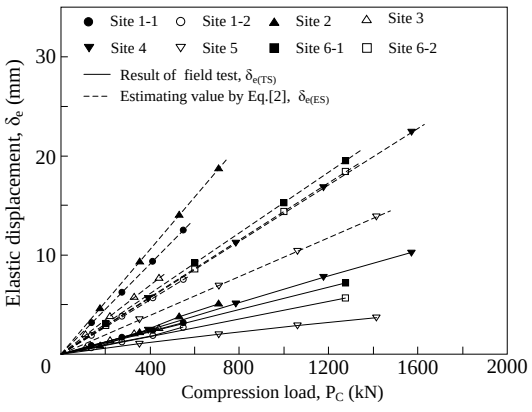

Fig. 11 Comparison of results of field test and Eq. (2)

Table 2 Errors between field tests and results of Eq. (2)

Site	Load (kN)	Field test	Estimated value by Eq. (2)		$\lvert\delta_{e(ES)} - \delta_{TC}\rvert$ (mm)	Error (%)
		δ_{TC} (mm)	$\delta_{e(TS)}$ (mm)	$\delta_{e(ES)}$ (mm)		
Site 1-1	560	4.665	3.209	12.784	9.57	74.4
Site 1-2	560	3.600	2.685	12.784	10.09	78.6
Site 2	720	7.232	5.240	19.472	14.23	72.6
Site 3	440	4.044	2.640	5.983	3.34	55.8
Site 4	1,570	13.644	10.224	22.873	12.65	55.3
Site 5	1,415	5.380	3.670	13.661	9.99	73.1
Site 6-1	1,275	9.945	7.221	13.133	5.91	51.4
Site 6-2	1,275	7.285	5.635	13.133	7.49	65.2

※ Error(%)=$\frac{\lvert\delta_{e(ES)}-\delta_{TC}\rvert}{\delta_{e(ES)}} \times 100$

※ For estimating $\delta_{e(ES)}$ by Eq.(2), E_{ST}=2.10×10^5(MPa) ; E_G=4732$\sqrt{\sigma_{ck}}$ (σ_{ck}=24MPa)

5.2 Correction factor n, in Eq. (9)

Based on the study results shown in Figs. 9 and 10, it was proposed to calculate the modified elastic settlement amount of the micropile structure as shown in Eq. (10). In order to calculate the modified elastic settlement amount, the correction factor n in Eq. (8) should be estimated.

Fig. 12 shows the value of factor n for each site obtained by analyzing the calculation result of Eq. (10) and the results of the field test, and the value of factor n for each site is as shown in Fig. 12(a). As shown in 12(a), the value of the coefficient n was approximately 0.12-0.16. Fig. 12(b) compares the value of factor n according to the change in the axial stiffness ratio of grout and steel bar, $(E_G \cdot A_G)/(E_{ST} \cdot A_{ST})$. As the axial stiffness ratio of the grout and steel bar increased, n tended to decrease nonlinearly as shown in Fig. 12(b). In addition, as shown in Fig. 12(c), when the relationship of $(E_G \cdot A_G)/(E_{ST} \cdot A_{ST})$-n was expressed in a semi-algebraic form, n tended to decrease linearly. Thereby, through the relationship of $\log_{10}[(E_G \cdot A_G)/(E_{ST} \cdot A_{ST})]$-n, the factor n can be defined as a function of the axial stiffness ratio of the grout and steel bar as follows.

$$n = f\left(\frac{E_G \cdot A_G}{E_{ST} \cdot A_{ST}}\right) = -0.065 \cdot log_{10}\left(\frac{E_G \cdot A_G}{E_{ST} \cdot A_{ST}}\right) + 0.135 \quad (12)$$

5.3 Settlement of the micropile structure, $\delta_{e(MES)}$

Fig. 13 compares the elastic settlement amount of the micropile structure, $\delta_{e(MES)}$, calculated in Eqs. (10) and (14) and the elastic displacement of micropile investigated through the field test (Fig. 9). As a result of comparison, it was found that the amount of settlement calculated through Eqs. (11) and (14) was slightly overestimated compared to the test results. Also, as shown in Table 3, the error for the two results was 4.2-43.9%, and the error was the largest at site 5.

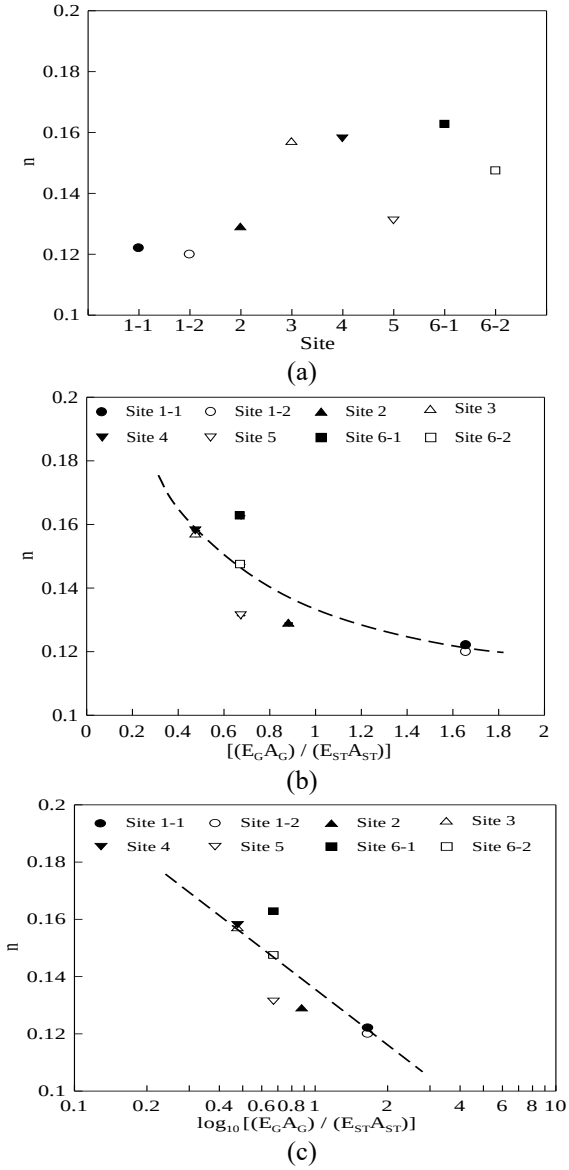

Fig. 12 Correction factor n of Eq. (9): (a) Coefficient n for each site, (b) Variation of n according to $(E_G \cdot A_G)/(E_{ST} \cdot A_{ST})$ and (c) Variation of n according to $\log_{10}((E_G \cdot A_G)/(E_{ST} \cdot A_{ST})$

Table 3 Elastic displacement differences and errors between field tests and estimated results of Eqs. (10) and (14)

Site	Load (kN)	Field test $\delta_{e(TS)}$ (mm)	Estimated value by Eq.(10) and (14)			$\lvert\delta_{e(MES)} - \delta_{e(TS)}\rvert$ (mm)	Error (%)
			$\frac{E_G \cdot A_G}{E_{ST} \cdot A_{ST}}$	n	$\delta_{e(MES)}$ (mm)		
Site 1-1	560	3.209	1.66	0.121	3.347	0.14	4.2
Site 1-2	560	2.685	1.66	0.121	3.347	0.66	19.7
Site 2	720	5.240	0.88	0.138	8.090	2.27	35.2
Site 3	440	2.640	0.48	0.156	2.902	0.37	9.00
Site 4	1,570	10.224	0.48	0.156	11.104	1.39	7.9
Site 5	1,415	3.670	0.67	0.148	6.524	2.87	43.9
Site 6-1	1,275	7.221	0.67	0.148	6.283	1.45	15.0
Site 6-2	1,275	5.635	0.67	0.148	6.283	0.13	10.2

※ Error(%)=$\frac{\lvert\delta_{e(MES)}-\delta_{e(TS)}\rvert}{\delta_{e(MES)}} \times 100$

※ For estimating $\delta_{e(MES)}$ by Eq.(12) and (16), E_{ST}=2.10×10^5(MPa) ; E_G=4732$\sqrt{\sigma_{ck}}$ (σ_{ck}=24MPa)

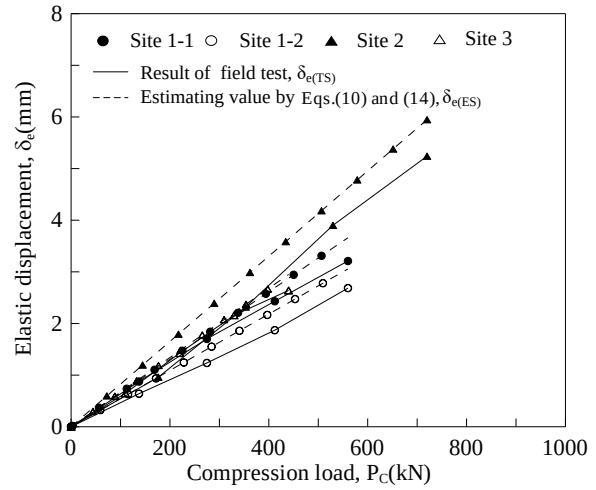

Fig. 13 Comparison of the estimated results of Eqs. (10) and (14) and $\delta_{e(TS)}$ of the test results: (a)Sites 1–3 and (b) Sites 4–6

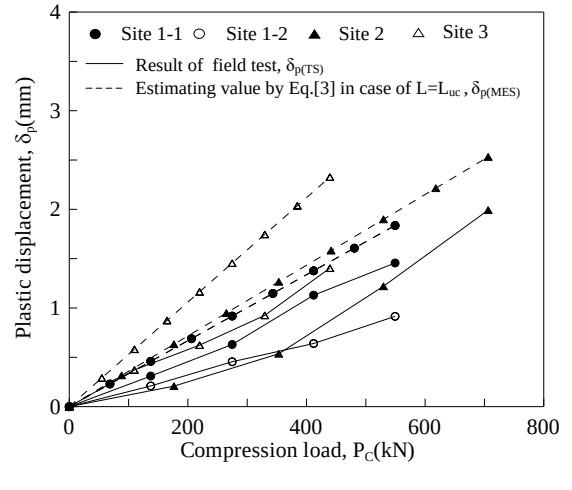

Fig. 14 Comparison of the estimated results of Eq. (3) with δ_p of the test results: (a) Sites 1–3 and (b) Sites 4–6

Likewise, as shown in Tables 2 and 3, the results of Eqs. (10) and (14) are closer to the field test results than the results of Eq. (2). This result is inconsistent with the prediction of the subsidence of the micropiles consisting of the grout and steel bars in Eq. (2), as in the existing piles of a single material. Thus, it shows that to predict the settlement amount of a micropile, a method for calculating the settlement amount of the pile considering the bearing and behavior characteristics of the micropile is required, such as that represented by Eqs. (10) and (14).

5.4 Settlment of the micropile shaft, $\delta_{P(MES)}$

Fig. 14 compares the settlement amount on the shaft of the micropile, $\delta_{p(MES)}$, calculated by substituting the uncased length(L→L_{uc}) in Eq. (3) and the plastic displacement of the micropile investigated through field tests. As shown in Fig. 14, when the amount of settlement was evaluated by substituting the uncased length for each site in Eq. (3), the calculation results were slightly overestimated compared to the plastic displacements of the micropiles investigated by the field test. Table 3 summarizes the displacement differences and errors obtained from the calculation results and test results when the uncased length is substituted. As a result of the

Table 4 Plastic displacement differences and errors between field tests and results of Eq. (3) in case of L=L_{uc}

Site	Load (kN)	Field test	Estimated value by Eq.(3) in case of L=L_{uc}			$\lvert\delta_{p(MES)} - \delta_{p(TS)}\rvert$ (mm)	Error (%)
		$\delta_{p(TS)}$ (mm)	L_{uc} (m)	E_s (kPa)	$\delta_{p(MES)}$ (mm)		
Site 1-1	560	1.456	5.0	60,000	1.836	0.38	11.4
Site 1-2	560	0.915	5.0	60,000	1.836	0.92	27.5
Site 2	720	1.992	5.0	60,000	2.531	0.54	21.3
Site 3	440	1.404	3.0	60,000	2.328	0.92	39.7
Site 4	1,570	3.420	4.0	100,000	3.995	0.57	14.4
Site 5	1,415	1.710	6.0	200,000	1.376	0.33	24.3
Site 6-1	1,275	2.724	5.0	60,000	4.262	1.54	36.1
Site 6-2	1,275	1.650	5.0	60,000	4.262	2.61	61.3

※ Error(%)=$\frac{\lvert\delta_{p(MES)}-\delta_{p(TS)}\rvert}{\delta_{p(MES)}} \times 100$

※ Elastic modulus of soil, E_s=1,200N (FHWA, 2005)

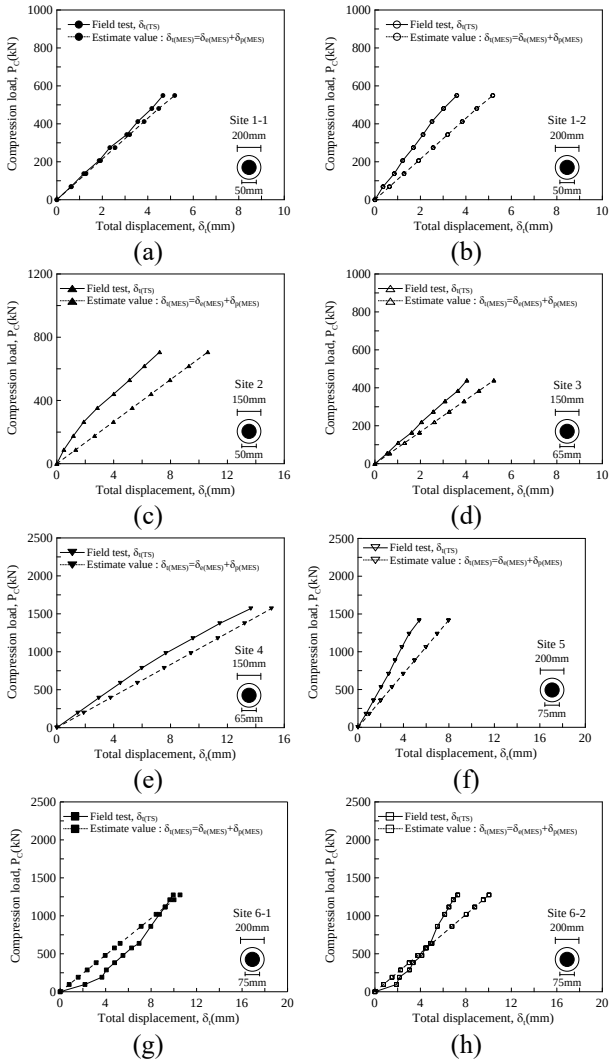

Fig. 15 Comparison of the estimated results of Eq. (11) the total displacement of the field test: (a) Site 1-1, (b) Site 1-2, (c) Site 2, (d) Site 3, (e) Site 4, (f) Site 5, (g) Site 6-1 and (h) Site 6-2

comparison, the displacement difference between $\delta_{p(MES)}$ and $\delta_{p(TS)}$ was about 0.33-2.61 mm, and the error was about 11.4-61.3%.

5.5 Total settlement of micropile, $\delta_{t(MES)}$

The results of Figs. 7 and 9 and 10 show that the bearing capacity of the micropile is equal to the sum of the resistance of the pile body and the skin friction resistance caused at the boundary of the ground/pile. In addition, through the study result in Fig. 13, it was shown that the elastic settlement amount of the micropile structure calculated by Eqs. (10) and (14) proposed in this study was found to be more consistent with the test results. Through the comparison results in Fig. 14, it was confirmed that it is appropriate to apply the uncased length in Eq. (3) when estimating the settlement amount of the micropile shaft. Therefore, it is possible to predict the total settlement amount of the micropile from the results of Figs. 13 and 14.

Table 5 Displacement differences and errors between $\delta_{t(MES)}$ and $\delta_{t(TS)}$

Site	Load (kN)	Field test	Estimated value			$\lvert\delta_{t(MES)} - \delta_{TC}\rvert$ (mm)	Error (%)
		δ_{TC} (mm)	$\delta_{e(MES)}$ (mm)	$\delta_{p(MES)}$ (mm)	$\delta_{t(MES)}$ (mm)		
Site 1-1	560	4.665	3.347	1.836	5.183	0.52	10.0
Site 1-2	560	3.600	3.347	1.836	5.183	1.58	30.5
Site 2	720	7.232	8.090	2.531	10.621	3.39	31.9
Site 3	440	4.044	2.902	2.328	5.229	1.19	22.7
Site 4	1,570	13.644	11.104	3.995	15.099	1.46	9.6
Site 5	1,415	5.380	6.524	2.466	8.990	3.61	31.9
Site 6-1	1,275	9.945	6.283	4.262	10.545	0.60	5.7
Site 6-2	1,275	7.285	6.283	4.262	10.545	3.26	30.9

※ Error(%)=$\frac{|\delta_{t(MES)}-\delta_{TC}|}{\delta_{t(MES)}} \times 100$

Fig. 15 compares the total settlement amount of the micropile, $\delta_{t(MES)}(=\delta_{e(MES)}+\delta_{p(MES)})$, evaluated through the results of Figs. 13 and 14 and the test results, $\delta_{t(TS)}$. As shown in Fig. 15, the total settlement amount of micropile, $\delta_{t(MES)}$, estimated through the prediction method proposed in this study was similar to or slightly overestimated from the total settlement amount investigated through field tests

Table 5 compares the displacement difference and error between the actual measured result and the predicted result. As a result of comparison, the displacement difference between $\delta_{t(MES)}$ and $\delta_{t(TS)}$ was 0.52-3.61 mm, and the error was 5.7-31.9%. In the case of the micropile of sites 2 and 5, the displacement difference and error were the largest, and the maximum displacement difference was 3.61 mm, and the maximum error was 31.9%. Thus, the results of Fig. 14 and Table 4 shows that the prediction method of micropile settlement proposed in this study can predict more reasonably than the existing prediction method. This can be known by comparing the test results with the calculation results according to the prediction method.

The comparison result in Table 2 compares the test result with the elastic settlement amount of the micropile structure predicted through Eq. (2), which is the existing method, and is a result of the settlement amount of the micropile shaft not being considered. Therefore, when comparing the total settlement amount, the displacement difference and error shown in Table 2 increase significantly.

On the other hand, the comparison results in Table 4 are the predicted total settlement amount of the micropile considering the settlement amount of the micropile structure and the shaft, and it can be seen that the predicted results and the test results were significantly reduced than the results in Table 2. Therefore, it is judged that the settlement amount can be predicted more rationally through the method proposed in this study.

6. Design considerations

The method proposed in this study should determine the settlement amount of the micropile structure using Eq. (10) before calculating the total settlement assessment amount. In Eq. (10), the elastic modulus and cross-sectional area of

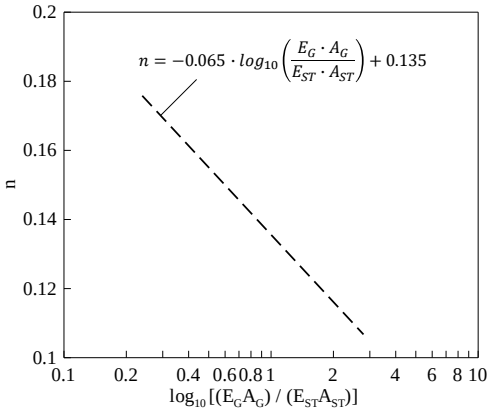

Fig. 16 Correction factor n of Eq. (9)

the steel bar, grout and micropile can be calculated using Eqs. (12) and (13). In addition, the correction factor, n must be determined. As shown in Fig. 12(c), since n is related to the axial stiffness ratio of the steel bar and the grout, the relationship of $(E_G \cdot A_G)/(E_{ST} \cdot A_{ST})$ and n can be defined as shown in Fig. 16. The correction factor n can be estimated through Fig. 16, and the modified coefficient, m', of Eq. (9) can be calculated.

As the behavior and support characteristics of the micropile were evaluated through on-site compression and tensile tests, it was reasonable to apply the uncased length of the micropile to the length in Eq. (3) when predicting the settlement amount of the micropile shaft. The total settlement amount of the micropile predicted from the method proposed in this study is slightly overestimated than the test result, but considering the conservative approach, it is judged more reasonable than the existing method.

7. Conclusions

Through field tests, it was confirmed that the load transfer characteristics of micropiles were different from those of existing piles, and that the main resistance to the working load was a steel bar among the micropile components. Considering the observed behavioral characteristics of micropiles, this study proposed a method for predicting the amount of elastic settlement of micropile structures. In addition, it was shown that it is reasonable to apply the uncased length of pile to the existing method when estimating the amount of settlement caused by the load acting on the shaft of the micropile predicted through the test result calculation method. The detailed results of this study are as follows.

1. The error between the settlement amount of the micropile predicted by the conventional method and the result investigated through the field test was approximately 50-80% (displacement difference = 3.3-14.0 mm), and it was not suitable for predicting the total settlement amount of the micropile.
2. When comparing the amount of settlement of the micropile predicted through the method proposed in this study and the field test results, the error between the two results was approximately 4-44% (displacement difference = 0.13-2.9 mm), which was significantly reduced compared to the estimated error through the existing method.
3. Through the field test results, it was confirmed that the amount of settlement caused by the load applied at the shaft of the micropile depends on the uncased length, L_{uc}. As a result of predicting the amount of settlement occurring on the shaft of the micropile considering this, the error with the test result was approximately 11-61%, and the amount of settlement could be predicted more rationally than when the total length of pile was applied.
4. The total settlement of piles obtained through the method for predicting the settlement of micropile proposed in this study had an error of 10-40% with the test result, and it was possible to predict the settlement of micropile more than the existing method.

The results of this study are proposed in consideration of the load-displacement relationship of the micropile investigated through field tests conducted at each site. Since the load transfer characteristics of the micropile may vary depending on the ground conditions around the pile and the cross-sectional area of the material constituting the micropile, detailed additional research is required.

References

ASTM D2487-06, "Standard Practics for Classification of Soils for Engineering Purpose(Unified Soil Classification System)", West Conshohocken, Pennsylvania, USA

CCTG (1992), "Technical Rules for the Design and Calculation of the Foundations of the Civil Engineering Works", Publication 62, Title V, France

Capatti, M.C., Dezi, F., Carbonari, S. and Gara, F. (2020), "Dynamic performance of a full-scale micropile group relevance of nonlinear behaviour of the soil adjacent to micropiles", *Soil Dyn. Earthq. Eng.*, **128**, 105858, https://doi.org/10.1016/j.soildyn.2019.105858.

Das, B.M. (2010), Principles of Foundation Engineering, (7th Edition), Cengage learning, Boston, MA, USA

El Kamash, W. and Han, J. (2017), "Numerical analysis of existing foundations underpinned by micropiles", *Int. J. Geomech.*, **17**(6), 04016126, https://doi.org/10.1061/(ASCE)GM.1943-5622.0000833.

El Kamash, W., El Naggar, H., Nabil, M. and Ata, A. (2020), "Optimizing the unconnected piled raft foundation for soft clay soils: numerical study", *J. Civil Eng. - KSCE*, **24**(4), 1095-1102, https://doi.org/10.1007/s12205-020-0567-3

FHWA (2005), "Micropiles design and construction", US Department of Transportation, Washington, DC, USA

Gómez, J., Cadden, A., Traylor, R.P. and Bruce, D.A. (2005), "Connection capacity between micropiles and existing footings-bond strength to concrete", *In Geo3 GEO Construction Quality Assurance/Quality Control Conference Proceedings*, Dallas, Fort worth, Texas, USA.

Hwang, T.H., Kim, K.H. and Shin, J.H. (2017a), "Bearing capacity of micropiled-raft system", *Struct. Eng. Mech.*, **63**(3), 417-428, https://doi.org/10.12989/sem.2017.63.3.417.

Hwang, T.H., Kim, K.H. and Shin, J.H. (2017b), "Effective installation of micropiles to enhance bearing capacity of micropiled raft", *Soils Found.*, **57**(1), 36-49, https://doi.org/10.1016/j.sandf.2017.01.003.

Han, J. and Ye, S.L. (2006), "A field study on the behavior of a foundation underpinned by micropiles", *Can. Geotech. J.*,

43(1), 30-42, https://doi.org/10.1139/t05-087.
Moradi, M.H., Keramati, M., Ramesh, A. and Naderi, R. (2021), "Experimental valuation of the effects of structural parameters installation methods and soil density on the micropile bearing capacity", *Int. J. Civil Eng.*, **19**(11), 1313-1325. https://doi.org/10.1007/s40999-021-00629-5.
Prakash, S. and Sharma, H.D. (1991), Pile Foundations in Engineering Practice, John Wiley & Sons, Washington, DC, USA
Vesic, A.S. (1977), Design of pile foundations. *NCHRP synthesis of highway practice*, **42**
Veludo, J., Júlio, E.N.B.S. and Dias-da-Costa, D. (2012), "Compressive strength of micropile-to-grout connections", *Constr. Build. Mater.*, **26**(1), 172-179. https://doi.org/10.1016/j.conbuildmat.2011.06.007.
Wang, C., Han, J.T. and Jang, Y.E. (2019),. "Experimental investigation of micropile stiffness affecting the underpinning of an existing foundation", *Appl. Sci.*, **9**(12), 2495. https://doi.org/10.3390/app9122495.
Xanthakos, P.P. (1991), Ground anchors and Anchored Structures, John Wiley & Sons, Washington, DC, USA.

GC